Surface-Stabilized Nonferromagnetic Ordering of a Layered Ferromagnetic Manganite

V. B. Nascimento,[1,*] J. W. Freeland,[2] R. Saniz,[3,†] R. G. Moore,[4] D. Mazur,[5] H. Liu,[4] M. H. Pan,[6] J. Rundgren,[7] K. E. Gray,[5] R. A. Rosenberg,[2] H. Zheng,[5] J. F. Mitchell,[5] A. J. Freeman,[3] K. Veltruska,[8] and E. W. Plummer[1,4]

[1]*Department of Physics and Astronomy, Louisiana State University, Baton Rouge, Louisiana 70803, USA*
[2]*Advanced Photon Source, Argonne National Laboratory, Argonne, Illinois 60439, USA*
[3]*Department of Physics and Astronomy, Northwestern University, Evanston, Illinois 60208-3112, USA*
[4]*Department of Physics and Astronomy, University of Tennessee, Knoxville, Tennessee, 37996-1200, USA*
[5]*Materials Science Division, Argonne National Laboratory, Argonne, Illinois 60439, USA*
[6]*Center for Nanophase Materials Sciences, Oak Ridge National Laboratory, Oak Ridge, Tennessee 37831, USA*
[7]*Theory of Materials, Department of Physics, Royal Institute of Technology, SE-106 91 Stockholm, Sweden*
[8]*Department of Surface and Plasma Science, Faculty of Mathematics and Physics, Charles University,*
V. Holesovickch 2, 18000 Prague 8, Czech Republic
(Received 24 June 2009; published 24 November 2009)

An outstanding question regarding the probing or possible device applications of correlated electronic materials (CEMs) with layered structure is the extent to which their bulk and surface properties differ or not. The broken translational symmetry at the surface can lead to distinct functionality due to the charge, lattice, orbital, and spin coupling. Here we report on the case of bilayered manganites with hole doping levels corresponding to bulk ferromagnetic order. We find that, although the hole doping level is measured to be the same as in the bulk, the surface layer is not ferromagnetic. Further, our low-energy electron diffraction and x-ray measurements show that there is a c-axis collapse in the outermost layer. Bulk theoretical calculations reveal that, even at fixed doping level, the relaxation of the Jahn-Teller distortion at the surface is consistent with the stabilization of an A-type antiferromagnetic state.

Because of the strong coupling between the lattice, electron, and spin in a strongly correlated material, it is not surprising that breaking the translational symmetry by creating a surface in a material can result in a new ground state at the surface. The more two-dimensional the transition metal oxide (TMO) is, the smaller the effect of creating a surface should be. Therefore, it is surprising that the (001) surface of the single-layered ruthenate, $Ca_{2-x}Sr_xRuO_4$, exhibits quite different properties compared with the bulk [1,2], including a purely electronic metal-insulator Mott transition for $x = 0.1$ [1] and a significant modification of the quantum critical point near $x_c \approx 0.5$ [2]. Another example is the $Fe_3O_4(001)$ surface, where a wavelike reconstruction stabilizes a polar-terminated surface and induces a half-metal to metal transition [3].

In the bulk, the bilayered TMO, $La_{2-2x}Sr_{1+2x}Mn_2O_7$, displays a variety of both magnetic and electronic states [4,5]. Changing the Sr/La concentration ratio results in a mixed valence state of Mn and gives rise to different ferromagnetic (FM), paramagnetic, and antiferromagnetic (AFM) phases. One could expect that the surface properties of a bilayered TMO might deviate from the bulk even more than in a single-layer TMO, e.g., $Ca_{2-x}Sr_xRuO_4$. Recently, there have been several studies of the electronic and magnetic properties, some of which support this hypothesis. Studies of the surface magnetic properties over the range of x from 0.36 to 0.40, for which the bulk is a FM metal, show the presence of a non-FM insulating behavior of the surface bilayer [6,7]. Angle-resolved photoemission

(ARPES) and tunneling studies have provided a direct look at the surface electronic structure at the Fermi level, E_F, to a depth of ≈ 1 nm, but the published results vary. For ARPES at $x = 0.40$, one group reports evidence for a pseudogap [8], while another group sees clear evidence for a strong quasiparticle peak [9], which tracks the electrical conductivity [10]. At slightly lower doping ($x = 0.36$–0.38), ARPES data show a more consistent picture with clear signs of a quasiparticle peak associated with the metallic state [11–13]. However, the physics of the bulk properties does not seem to change significantly in this doping range (0.36–0.40), leaving open the question of why the surface properties vary so significantly. Gold-tip point-contact tunneling (at $x = 0.36$) concludes there is an insulating surface bilayer acting as a tunnel barrier [6] and shows evidence for a metallic second bilayer with the expected suppression of the density of states near E_F due to Coulomb interactions [14]. However, scanning tunneling spectroscopy for the $x = 0.3$ surface concludes that a pseudogap dominates the tunneling characteristics [15].

The aim of this work is to understand the nature of the structure-functionality relationship at the surface of correlated electronic materials (CEMs), specifically the origin of the non-FM phase present at the (001) surface of the $La_{2-2x}Sr_{1+2x}Mn_2O_7$ manganites by a combined experimental and theoretical analysis. For this, a quantitative study of surface structure was performed using LEED [16], determining geometric and chemical ordering. The full-potential linearized augmented plane-wave (FLAPW) theoretical approach [17] was employed to calculate the

electronic structure of the $La_{2-2x}Sr_{1+2x}Mn_2O_7$ system. Further, electronic and magnetic characterizations of *in situ* cleaved (001) surfaces were performed using x-ray resonant magnetic scattering (XRMS).

Single-crystal samples of $La_{1.28}Sr_{1.72}Mn_2O_7$ ($x = 0.36$) and $La_{1.2}Sr_{1.8}Mn_2O_7$ ($x = 0.40$) were cleaved *in situ* under ultrahigh vacuum conditions at temperatures of 80 and 300 K. The following LEED and x-ray studies yielded the same results regardless of the cleaving temperature. The LEED structural analyses indicate a LaSrO rocksalt-terminated surface, as expected for the cleavage of these layered manganites, in agreement with other recent studies of the bilayer surface [15,18]. The observed diffraction patterns presented a (1 × 1) structure with $p4mm$ symmetry [Fig. 1(a)] and no indication of surface reconstruction, as had been previously suggested as a possible root cause for altered surface properties [6]. This indicates that the changes in the physical properties at the surface must be due to a change not of the symmetry, but could be due to a change of lattice parameters at the surface.

To probe the details of the surface structure, a quantitative analysis of the LEED $I(V)$ data was conducted. Variations in the diffraction intensity as a function of the incident electron beam energy [$I(V)$] are connected to the details of the surface structure [16]. Symmetrically equivalent beams, according to the $p4mm$ symmetry, were then averaged leading to 11 nonequivalent beams [$I(V)$ curves]:
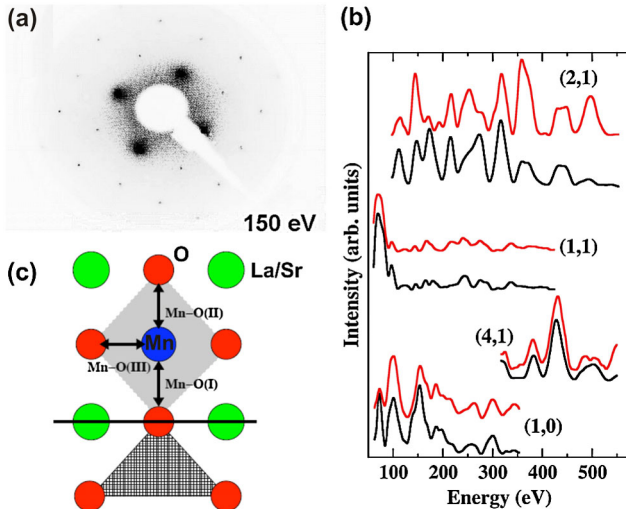

FIG. 1 (color online). (a) LEED diffraction pattern for the $x = 0.36$ sample at 150 eV. (b) LEED: comparison between theoretical and experimental $I(V)$ curves for the $x = 0.40$ system at a temperature of 300 K. Red (gray) and black lines correspond, respectively, to the theoretical and experimental intensities. $I(V)$ curves for four distinct diffracted beams [(1,0), (1,1), (2,1), and (4,1)] are presented. (c) Top half of the first bilayer, showing the three distinct manganese-oxygen distances: (1) Mn-O(I), distance between manganese and oxygen in the center of the bilayer; (2) Mn-O(II), distance between manganese and top/bottom oxygen; (3) Mn-O(III), distance between manganese and in-plane oxygen.

(1,0), (1,1), (2,0), (2,2), (2,1), (3,0), (3,1), (3,3), (4,0), (4,1), and (3,2), in total energy ranges of 3129 and 3509 eV, respectively, for the $x = 0.36$ and 0.40 samples at 300 K. Optimization of the (001) surface structure of both the $x = 0.36$ and 0.40 systems, within the constraints of $p4mm$ symmetry, was performed by searching for the minimum of the Pendry R factor (R_P) [19], which was employed to quantify the theory-experiment agreement. Considering the complexity of the structure of these systems, excellent final theory-experiment agreements were achieved, as characterized by the final R_P values of 0.18 and 0.20 for $x = 0.36$ and 0.40, respectively, at 300 K.

A comparison between typical experimental and theoretical $I(V)$ curves obtained for the $x = 0.40$ best structure can be seen in Fig. 1(b). Both $x = 0.36$ and 0.40 (001) surfaces present the same final structure within the accuracy of the results. An analysis of experimental data collected at 80 K indicates no change in the surface structure for either doping level at reduced temperature. The main structural features of the (001) surface pertain to changes in the three different Mn-O distances in the top half of the surface bilayer, which are defined in Fig. 1(c) and presented in Table I. Notice that the most significant change is a contraction of the Mn-O(II) spacing at the surface, while the Mn-O(I) and Mn-O(III) spacings basically keep their bulk values (within uncertainties). This change in the Mn-O(II) distance will be seen below to play a key role in the physical properties of the surface. Of particular importance is the distortion of the octahedra, known as a Jahn-Teller distortion, which alters the energies of the Mn $3d$ orbitals. The Jahn-Teller distortion (Δ_{JT}) can be defined as the ratio of the averaged apical Mn-O distances [Mn-O(I) and Mn-O(II)] to the equatorial Mn-O distance [Mn-O(III)]: $\Delta_{JT} = [Mn\text{-}O(I) + Mn\text{-}O(II)]/[2 \times Mn\text{-}O(III)]$.

According to the experimental results of the bulk structure [20,21], Δ_{JT} decreases from ≈ 1.034 at $x = 0.30$ (FM) to ≈ 1.011 at $x = 0.50$ (AFM). The change in magnetic order with increasing hole concentration (x) results from the depopulation of the $3z^2 - r^2$ orbitals and is coupled to a decrease in Δ_{JT} [22]. This weakens the ferromagnetic double exchange between the bilayers in favor of the t_{2g} AFM superexchange, resulting in an A-type state with moments aligned ferromagnetically within the layer and antiparallel between the double layers.

As previously mentioned, the surface structural results show that both the Mn-O(I) and Mn-O(III) distances exhibit bulklike values for both samples and that Mn-O(II) is systematically reduced in the surface. The reduction of Mn-O(II) is consistent with a change in the orbital occupancy and, consequently, the magnetic order at the surface, as will be discussed below. Using bulk values for Mn-O(I) and Mn-O(III) [20], one can yield Δ_{JT} equal to (1.0013 ± 0.0155) and (1.0044 ± 0.0181) at the surface for $x = 0.36$ and 0.40, respectively. If a comparison with bulk is made, one may speculate that both systems present AFM order at the surface, possibly of an A type. Specifically, the surface

TABLE I.   The distances between Mn and the three different types of O [top, middle, and plane, as shown in Fig. 1(c) in the top half of the first bilayer] are presented: Mn-O(I), Mn-O(II), and Mn-O(III). The ratios between Mn-O(I) and Mn-O(II) distances, as well as the Jahn-Teller distortion (Δ_{JT}), are also shown. The surface values presented correspond to a temperature of 300 K.

Parameter	$x = 0.36$	$x = 0.40$	$x = 0.35$ (bulk) [20]	$x = 0.40$ (bulk) [21]
Mn-O(I)	(1.952 ± 0.09) Å	(1.953 ± 0.09) Å	1.929 Å	1.936 Å
Mn-O(II)	(1.924 ± 0.06) Å	(1.936 ± 0.07) Å	2.010 Å	2.003 Å
Mn-O(III)	(1.937 ± 0.02) Å	(1.937 ± 0.02) Å	1.929 Å	1.9339 Å
Mn-O(I)/Mn-O(II)	(1.014 ± 0.032)[a]	(1.008 ± 0.036)[a]	0.959 70	0.966 55
Δ_{JT}	(1.0013 ± 0.0155)[a]	(1.0044 ± 0.0181)[a]	1.0210	1.018 37

[a]Because Mn-O(I) and Mn-O(III) distances do not change at the surface (within uncertainties), bulk values have been adopted for Mn-O(I) and Mn-O(III).

relaxation produces a collapse in the c axis, decreasing the Jahn-Teller distortion and, in analogy with the bulk results, driving the system from FM to AFM order.

To connect to the previous work showing the loss of FM order at the surface and the concomitant formation of an insulating surface bilayer [6,7], we did a direct comparison of the surface magnetism for crystals cleaved in air and *in situ*. First, we examined in detail the electronic properties of Mn near the surface as probed by x-ray absorption spectroscopy. We compared the surface-sensitive absorption (electron yield) for the *in situ* versus *ex situ* cleaving and found that they are identical, indicating that the electronic structure of the Mn atoms in the surface bilayer is largely unaffected by the cleaving environment [see Fig. 2(a)]. As shown in Fig. 2(b), a comparison with absorption measurements in the surface and bulk sensitive modes, it is clear that the surface has the same composition as the bulk. Through *in situ* x-ray photoelectron spectroscopy (not shown), we find no evidence of Sr segregation to the surface, which is in agreement with x-ray absorption, LEED, and previous studies for layered manganites [18].

The magnetic state at the surface was probed directly by measuring the polarization-dependent magnetic reflectivity, referred to as XRMS. The XRMS results from an interference between the charge and magnetic scattering from the chemical and magnetic profiles. Using the results above that show a uniform chemical profile, this interference can be measured via angle-dependent XRMS and can determine the nature of the magnetism near the surface or interface [6,7]. The key observation from the XRMS measurements is that the change of sign of the XRMS signal occurs and can be connected to a single surface bilayer which displays no net magnetism and is therefore not ferromagnetic like the bulk. Such a sign change would be absent in the case where the ferromagnetism was present in the surface bilayer [7]. In Fig. 2, we present a comparison between an *in situ* (c) and *ex situ* (d) cleaved sample measured under the same conditions. It is clear that the data for both surfaces show the same sign reversal, previously shown to be due to a non-FM surface bilayer. Having shown the similarity between the electronic and magnetic behavior of the two surface preparations allows

us to conclude that this is the intrinsic physical property of the surface bilayer.

As previously discussed, there is a strong correlation between crystal structure and physical properties, the structure-functionality relationship, in a TMO system such as $La_{2-2x}Sr_{1+2x}Mn_2O_7$. Therefore, a detailed knowledge of the surface structure is required for understanding the physical properties at the surface. The experimentally determined surface structure indicates a change in the Mn-O(II) distance of the top half of the first bilayer, as can be seen in Table I, where surface as well as bulk values for these bond lengths are presented. The Mn-O(I) and Mn-O(III) distances remain basically bulklike. In spite of the uncertainties in their values, the experimental results systematically and consistently indicate the same behavior for both the $x = 0.36$ and 0.40 systems. The magnetic and electronic properties of the bilayered manganites are strongly related to the Mn-O distances and, consequently,
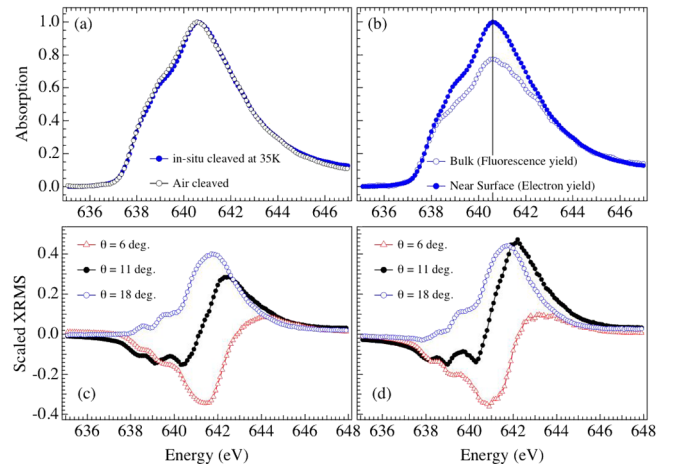

FIG. 2 (color online).   (a) Comparison of surface-sensitive x-ray absorption (electron yield) for *in* versus *ex situ* cleaving showing identical surface electronic structure for the two different surface preparations. (b) Comparison of surface versus bulk absorption showing similar composition for both regions. X-ray resonant magnetic scattering (XRMS) as a function of angle for (c) *in situ* and (d) *ex situ* cleaved samples. The sign reversal is attributed to a non-FM surface bilayer and is clearly seen in both cases, indicating that this is an intrinsic property of the surface layer.
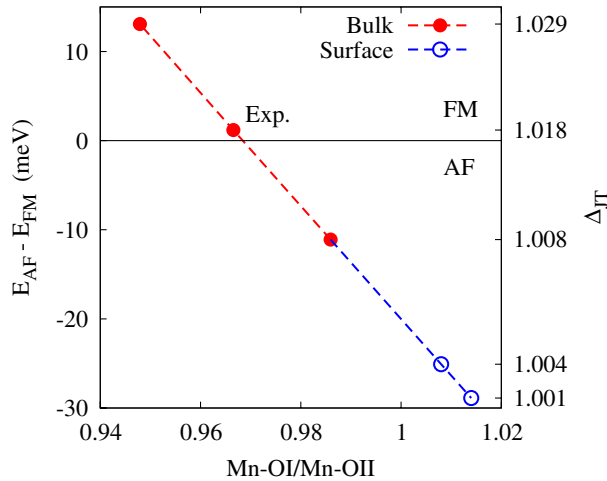
FIG. 3 (color online).   FLAPW for $x = 0.4$ (bulk). The total energy difference between AF and FM configurations ($\Delta E = E_{AF} - E_{FM}$) is presented as the Mn-O(I)/Mn-O(II) ratio varied by changing the Mn-O(II) distance. The associated Jahn-Teller distortion (Δ_{JT}) is also presented. The bulk experimental values for $x = 0.40$, as well as the surface values for $x = 0.36$ and 0.40, are presented in the graph.

with the associated Jahn-Teller distortion. As previously discussed, a comparison with bulk results strongly suggests an AFM phase at the surface [20], a conclusion supported by surface-sensitive magnetic measurements [6,7].

Theoretical calculations were performed on a bulk system to explore the structure-functionality relationship, specifically how the magnetic order correlates with Mn-O octahedron distortion at a fixed hole concentration. The calculations were performed with the FLAPW implementation [17] of the density-functional approach to the electronic structure and properties of crystalline solids. Our theoretical results for hole doping corresponding to $x = 0.40$, using as our initial structural parameters those of Mitchell et al. [21], are presented in Fig. 3. The total energy difference between AFM and FM configurations ($\Delta E = E_{AFM} - E_{FM}$) is presented in the following situation: the Mn-O(I)/Mn-O(II) ratio is varied by changing the Mn-O(II) distance. Positive or negative values for ΔE indicate a FM or AFM state, respectively. For comparison with Table I, the right panel presents the correspondence between the MnO(I)/Mn-O(II) ratio and the Jahn-Teller distortion. The experimental values at the surface for the Mn-O(I)/Mn-O(II) ratio are presented in Table I for both $x = 0.36$ and 0.40 surfaces. As can be seen in Table I and in Fig. 3, the surface Mn-O(I)/Mn-O(II) ratios obtained by LEED of 1.004 for $x = 0.40$ and 1.001 for $x = 0.36$ would both drive the system into an AFM phase. The theoretical predictions presented in Fig. 3 predict a 25-meV stabilization for the AFM-ordered phase at the surface. Significantly, as in the bulk, it is the Jahn-Teller distortion that seems to correlate strongly with magnetic order. The behavior of $\Delta E = E_{AFM} - E_{FM}$ with changes in Δ_{JT} is

clear from Fig. 3. A weaker Jahn-Teller distortion systematically indicates a tendency to an AFM phase. As can be inferred from Table I, the empirical Δ_{JT} surface values obtained by LEED analyses indicate an AFM phase as the most stable state. These results are in agreement with the bulk experimental work by Kubota et al. [20].

Further details about the methodologies adopted in this Letter are presented elsewhere [23].

*Corresponding author.
vnascimento@lsu.edu
†Present address: Departement Fysica, Universiteit Antwerpen, B-2020 Antwerpen, Belgium.

[1] R. G. Moore et al., Science **318**, 615 (2007).
[2] R. G. Moore et al., Phys. Rev. Lett. **100**, 066102 (2008).
[3] R. Pentcheva et al., Surf. Sci. **602**, 1299 (2008).
[4] T. Kimura et al., Science **274**, 1698 (1996).
[5] J. F. Mitchell et al., J. Phys. Chem. B **105**, 10 731 (2001).
[6] J. W. Freeland et al., Nature Mater. **4**, 62 (2005).
[7] J. W. Freeland et al., J. Phys. Condens. Matter **19**, 315210 (2007).
[8] Y. D. Chuang et al., Science **292**, 1509 (2001).
[9] N. Mannella et al., Nature (London) **438**, 474 (2005).
[10] N. Mannella et al., Phys. Rev. B **76**, 233102 (2007).
[11] Z. Sun et al., Phys. Rev. Lett. **97**, 056401 (2006).
[12] S. de Jong et al., Phys. Rev. B **76**, 235117 (2007).
[13] Z. Sun et al., Nature Phys. **3**, 248 (2007).
[14] D. Mazur et al., Phys. Rev. B **76**, 193102 (2007).
[15] H. M. Ronnow et al., Nature (London) **440**, 1025 (2006).
[16] M. A. Van Hove, W. H. Weinberg, and C.-M. Chan, *Low-Energy Electron Diffraction Experiment, Theory, and Surface Structure Determination* (Springer-Verlag, Berlin, 1986).
[17] E. Wimmer, H. Krakauer, M. Weinert, and A. J. Freeman, Phys. Rev. B **24**, 864 (1981); H. J. F. Jansen and A. J. Freeman, *ibid.* **30**, 561 (1984).
[18] F. Loviat et al., Nanotechnology **18**, 044020 (2007).
[19] J. B. Pendry, J. Phys. C **13**, 937 (1980).
[20] M. Kubota et al., J. Phys. Soc. Jpn. **69**, 1606 (2000).
[21] J. F. Mitchell et al., Phys. Rev. B **55**, 63 (1997).
[22] K. Hirota et al., Phys. Rev. B **65**, 064414 (2002).
[23] See EPAPS Document No. E-PRLTAO-103-028949 for more details about the experimental and theoretical approaches. For more information on EPAPS, see http:// www.aip.org/pubservs/epaps.html.